

Effect of finite correlation time of frequency modulation on resonance Raman scattering and luminescence

T. Takagahara

Electrical Communications Laboratories, Nippon Telegraph and Telephone Corporation, Musashino-shi, Tokyo 180, Japan

(Received 31 July 1986)

The effects of the finite correlation time of the external modulation on the secondary-emission spectra are clarified emphasizing the deviation from the motional narrowing limit or the impact approximation in the case of large off-resonance excitation. The dependences of the excitation spectrum of the secondary emission on the modulation parameters and on the inhomogeneous broadening are studied systematically. It is found that the excitation spectrum of the luminescence shows a faster decrease than that of the Raman scattering as the off-resonance frequency increases. The present theory is relevant for explaining the recent experiment by Watanabe, Kinoshita, and Kushiida [Chem. Phys. Lett. **126**, 197 (1986)] on the β -carotene in solutions. A general theory of the time-resolved spectra of the secondary emission is formulated to incorporate the effect of the finite correlation time. The luminescence component shows a slow temporal decay with the longitudinal relaxation rate. It is found for the first time that the difference is unexpectedly large between the transient behavior of the luminescence intensity and that of the intermediate-state population for the slow-modulation regime and that the difference indicates the effect of finite correlation time of the frequency modulation. On the other hand, the transient behavior of the Raman scattering contains a fast component that follows the envelope of the excitation-pulse intensity and the same slow component as the luminescence. The ratio of the slow component to the total intensity depends sensitively on the modulation parameters and the off-resonance frequency. The modulation parameters of the system in question can be estimated from these dependences in combination with the spectral characteristics of the emission under stationary excitation.

I. INTRODUCTION

Recently the excitation spectra for Raman scattering and luminescence have been measured systematically on the β -carotene in solutions.¹ It has been found that the excitation spectra for the two components show quite different behaviors. This cannot be explained by the theory of secondary emission in the motional narrowing limit since the theory gives the same excitation spectra for both components.²⁻⁴ However, the difference in the excitation spectra for the Raman scattering and for the luminescence was already predicted in the initiative work on the second-order optical processes by Takagahara, Hanamura, and Kubo.² The main concerns there were how the quantum coherence between the light absorption and emission is affected by the relaxation processes in the intermediate state and how the coexistence ratio of the Raman scattering and the luminescence is determined by the relaxation constants and the off-resonance energy. Various kinds of stochastic models were developed to simulate the intermediate-state interaction.^{2,3} In the stochastic theory, the total system is divided into a relevant system and an environmental system or reservoir. The effect of the latter on the relevant system is taken into account in terms of random forces and the reservoir is considered to be always in thermal equilibrium since it has a large number of degrees of freedom. The system of β -carotene in solutions is a typical example to which our stochastic theory can be applied suitably. The relevant system in this case is the β -carotene molecule itself, and the reser-

voir comprises the solvent molecules surrounding the β -carotene molecule. The solvent molecules modulate the energy levels of the β -carotene molecule through molecular interaction. On the other hand, the β -carotene molecule has a strong optically allowed transition from the 1A_g ground state to the 1B_u excited state.¹ Thus, the second-order optical process relevant to the experiments of Ref. 1 is the transition from 1A_g to 1A_g through the 1B_u level leaving some combinations of vibrational modes of the β -carotene molecule. This process can be modeled by a three-level system in which the energy of the intermediate state is modulated randomly by the environment.

The stochastic theory of second-order optical processes by Takagahara, Hanamura, and Kubo^{2,3} can describe the overall features of coexistence of the Raman scattering and the luminescence from the static (statistical) regime to the motional narrowing regime in a unified manner. The key parameters in the stochastic theory are the amplitude Δ_m and the rate γ_m of the frequency modulation. The static (statistical) regime is usually characterized by a large value of Δ_m/γ_m corresponding to the slow-modulation case, i.e., small γ_m , or the strong-coupling case, i.e., large Δ_m . On the other hand, the motional narrowing regime is characterized by a small value of Δ_m/γ_m corresponding to the fast-modulation case or the weak-coupling case. The excitation spectra for the Raman scattering and for the luminescence show various features depending on the ratio Δ_m/γ_m . From the comparison of experimental data with our theory, Watanabe *et al.*¹ estimated the ratio Δ_m/γ_m to be about 3 for the

β -carotene in isopentane. This value indicates that this system belongs to the slow-modulation regime and that the effect of the finite correlation time of frequency modulation cannot be neglected.

In this paper, a new method is proposed for calculating the secondary-emission spectra in a unified manner from the static regime to the motional narrowing regime. The newly devised method is quite efficient and time saving for numerical computation. At the same time, it is found that the factorization approximation introduced by Mukamel¹ is not justified in the slow-modulation regime. The excitation profiles of the Raman scattering and of the luminescence are calculated by use of the newly devised method and their dependence on the parameter ratio Δ_m/γ_m is clarified.

On the other hand, the time response of the Raman scattering and the luminescence reflects most directly the dynamics of the relevant system and is important in elucidating the relaxation processes.⁵⁻⁷ Here, a general formalism is developed to calculate the time-resolved emission spectra from the slow-modulation regime to the motional narrowing regime. The typical dependences of the time response of the Raman scattering and the luminescence on the parameter ratio Δ_m/γ_m are clarified and some methods to estimate the modulation parameters are proposed.

The effect of the finite correlation time of the frequency modulation becomes emphasized in the case of large off-resonance excitation since the duration when the system is staying in the excited state is roughly on the order of $(\Delta\omega)^{-1}$ where $\Delta\omega$ is the off-resonance energy of the excitation light. When this period is comparable to the correlation time, the treatment in the motional narrowing limit becomes invalid.⁸ It is to be noted that the effect of the finite correlation time appears not only in the second-order optical processes but also in other nonlinear optical phenomena. One of the most significant examples is the breakdown of the optical Bloch equation in the coherent transient phenomena discovered recently by DeVoe and Brewer.⁹ In this case, the characteristic time of the system is the Rabi oscillation period and this becomes comparable to the correlation time of frequency modulation when the incident light intensity is increased, resulting in

the breakdown of the optical Bloch equation. Thus the effect of the finite correlation time of frequency modulation manifests itself in a wide class of dynamical relaxation phenomena.

II. EMISSION SPECTRUM UNDER GAUSSIAN-MARKOVIAN FREQUENCY MODULATION

As mentioned in the Introduction, the energy levels of the β -carotene molecule in solutions are modulated by the thermal motion of the surrounding solvent molecules. The number of solvent molecules participating in the frequency modulation is quite large and thus the stochastic property of the frequency modulation can be regarded as a Gaussian process as a consequence of the central-limit theorem. Furthermore, the Markovian property can be assumed for simplicity. The model system of interest is described by a three-level system in which only the excited or intermediate state suffers a random frequency modulation. The relevant Hamiltonian is written as

$$H = |a\rangle E_a \langle a| + |b\rangle [E_b + x(t)] \langle b| + |c\rangle E_c \langle c|, \quad (2.1)$$

where a , b , and c denote the ground state, the excited state, and the final state with corresponding energy E_j ($j=a, b, c$), respectively. The random frequency modulation $x(t)$ is a Gaussian-Markovian process with zero mean value,³ i.e.,

$$\langle x(t) \rangle = 0, \quad (2.2)$$

and

$$\langle x(t_1)x(t_2) \rangle = \Delta_m^2 \exp(-\gamma_m |t_1 - t_2|), \quad (2.3)$$

where Δ_m and γ_m denote the amplitude and rate of the frequency modulation, respectively. The light scattering process can be described by a second-order perturbation with respect to the interaction with the radiation field.² The probability amplitude corresponding to the light scattering process, in which an incident photon with frequency ω_1 is absorbed and a photon with frequency ω_2 is emitted, is given by the expression

$$\psi^{(2)}(t) = \int_0^t dt_1 \int_0^{t_1} dt_2 e^{-i\omega_1 t_2 + i\omega_2 t_1} \langle c | e^{-iH(t-t_1)} V_{cb} e^{-iH(t_1-t_2)} V_{ba} e^{-iHt_2} | a \rangle, \quad (2.4)$$

where V_{ij} is the transition matrix element of the electromagnetic interaction Hamiltonian between the $|i\rangle$ and $|j\rangle$ states and the Planck constant \hbar will be put to be unity in the following. The time-development operator $\exp(-iHt)$ should be interpreted as an ordered exponential since the Hamiltonian is time dependent. The emission spectrum $I(\omega_1, \omega_2)$ is identified with the transition probability per unit time, i.e.,

$$I(\omega_1, \omega_2) = \lim_{t \rightarrow \infty} \frac{d}{dt} \langle |\psi^{(2)}(t)|^2 \rangle, \quad (2.5)$$

where the angular brackets denote the average over the stochastic variable $x(t)$. Accordingly, apart from unimportant factors, it is found that

$$I(\omega_1, \omega_2) = \text{Re}[A_I + A_{II} + A_{III}], \quad (2.6)$$

with the terms

$$A_I = \int_0^\infty d\tau \int_0^\infty d\tau' \int_0^\infty d\mu \exp\{-(\gamma_b + \gamma_c - i\Delta\omega_2)\tau - (\gamma_b + i\Delta\omega_1)\tau' - [\gamma_c + i(\Delta\omega_1 - \Delta\omega_2)]\mu - f_-(\tau, \tau', \mu)\}, \quad (2.7)$$

$$A_{II} = \int_0^\infty d\tau \int_0^\infty d\tau' \int_0^\infty d\mu \exp[-(\gamma_b + \gamma_c - i\Delta\omega_2)\tau - (\gamma_b + i\Delta\omega_1)\tau' - 2\gamma_b\mu - f_-(\tau, \tau', \mu)] , \quad (2.8)$$

$$A_{III} = \int_0^\infty d\tau \int_0^\infty d\tau' \int_0^\infty d\mu \exp[-(\gamma_b + \gamma_c - i\Delta\omega_2)\tau - (\gamma_b - i\Delta\omega_1)\tau' - 2\gamma_b\mu - f_+(\tau, \tau', \mu)] , \quad (2.9)$$

and with

$$f_\pm(\tau, \tau', \mu) = \Delta_m^2 [\phi(\tau) + \phi(\tau') \pm e^{-\gamma_m\mu}(1 - e^{-\gamma_m\tau})(1 - e^{-\gamma_m\tau'})] / \gamma_m^2 , \quad (2.10)$$

and

$$\phi(\tau) = e^{-\gamma_m\tau} + \gamma_m\tau - 1 , \quad (2.11)$$

where $\Delta\omega_1 = \omega_1 - (E_b - E_a)$ and $\Delta\omega_2 = \omega_2 - (E_b - E_c)$ and the damping constants γ_b and γ_c denote half of the population decay rates of the $|b\rangle$ and $|c\rangle$ levels, respectively. The three terms A_I , A_{II} , and A_{III} correspond to the choice of the chronological order among the time variables t_1 , t_2 , t'_1 , and t'_2 , and τ , τ' , and μ are the time intervals as shown in Fig. 1.

Now, the way to evaluate the following integral is discussed. In the expression

$$\int_0^\infty d\tau \int_0^\infty d\tau' \int_0^\infty d\mu \exp[-\sigma\tau - \sigma'\tau' - z\mu - a(e^{-\gamma\tau} + \gamma\tau - 1) - a(e^{-\gamma\tau'} + \gamma\tau' - 1) \pm ae^{-\gamma\mu}(1 - e^{-\gamma\tau})(1 - e^{-\gamma\tau'})] , \quad (2.12)$$

σ , σ' , and z stand for the constants appearing in (2.7)–(2.9). γ_m is abbreviated as γ , and $a = \Delta_m^2 / \gamma_m^2$. In the previous publication,³ the last exponent in (2.12) was expanded and the μ integral was calculated first. This expansion is rapidly convergent for the motional narrowing regime because $a = \Delta_m^2 / \gamma_m^2$ is small, whereas it is not efficient for the slow modulation regime since the expansion parameter a becomes quite large. Hence, a more general formalism is required to cover the whole range of the parameter ratio Δ_m / γ_m . For that purpose, the scaling of variables t and t' is introduced as

$$\tau = u / \Delta_m, \quad \tau' = u' / \Delta_m , \quad (2.13)$$

and the integral in (2.12) is rewritten as

$$\Delta_m^{-2} \int_0^\infty du \int_0^\infty du' \int_0^\infty d\mu \exp[-\bar{\sigma}u - \bar{\sigma}'u' - z\mu - a(e^{-pu} + pu - 1) - a(e^{-pu'} + pu' - 1) \pm e^{-\gamma\mu}ug(u)u'g(u')] , \quad (2.14)$$

where $g(u) = (1 - e^{-pu}) / pu$, $p = \gamma_m / \Delta_m$, $a = p^{-2}$, $\bar{\sigma} = \sigma / \Delta_m$, and $\bar{\sigma}' = \sigma' / \Delta_m$. The function $g(u)$ decreases monotonically and is less than unity irrespective of the value of p . Thus the last exponent in (2.14) can be expanded without a large factor and the result is given by the expression

$$\Delta_m^{-2} \sum_{n=0}^{\infty} \frac{(\pm 1)^n}{n!} \frac{1}{z + n\gamma_m} \int_0^\infty du [ug(u)]^n \exp[-\bar{\sigma}u - a(e^{-pu} + pu - 1)] \\ \times \int_0^\infty du' [u'g(u')]^n \exp[-\bar{\sigma}'u' - a(e^{-pu'} + pu' - 1)] . \quad (2.15)$$

The integrals in (2.15) have a simple expression in the continued-fraction representation, as given in Appendix A. This formalism is effective over the entire range of the parameter ratio, $p = \gamma_m / \Delta_m$, and can describe the change in the secondary emission spectrum in a unified manner from the slow-modulation regime to the motional narrowing regime.

Typical secondary-emission spectra calculated by the above formalism are shown in Fig. 2. Here the validity of the factorization approximation introduced by Mukamel⁴ is also examined. It will be shown that the factorization approximation cannot be justified in the slow-modulation regime since the correlation time of the random frequency modulation is long and the average of the product of three Green functions cannot be decoupled into the product of three independently averaged Green functions.⁴ The factorization approximation corresponds to retaining only the first term ($n = 0$) out of the summation in (2.15), namely,

$$\int_0^\infty d\tau \int_0^\infty d\tau' \int_0^\infty d\mu \exp[-\sigma\tau - \sigma'\tau' - z\mu - a(e^{-\gamma_m\tau} + \gamma_m\tau - 1) - a(e^{-\gamma_m\tau'} + \gamma_m\tau' - 1) \\ \pm ae^{-\gamma_m\mu}(1 - e^{-\gamma_m\tau})(1 - e^{-\gamma_m\tau'})] \\ \rightarrow \Delta_m^{-2} z^{-1} \int_0^\infty du \exp[-\bar{\sigma}u - a(e^{-pu} + pu - 1)] \int_0^\infty du' \exp[-\bar{\sigma}'u' - a(e^{-pu'} + pu' - 1)] . \quad (2.16)$$

Here the integrals with respect to u and u' give rise to the emission and absorption spectra in the linear response theory, respectively. The factor z is $\gamma_c + i(\Delta\omega_1 - \Delta\omega_2)$ for the term A_I and $2\gamma_b$ for both terms A_{II} and A_{III} . When

$\gamma_m \gg \gamma_b$ and γ_c , namely, in the motional narrowing regime, the contribution from the terms for nonzero n 's in (2.15) can be safely neglected. On the other hand, in the slow-modulation regime where γ_b and $\gamma_c \gg \gamma_m$ the con-

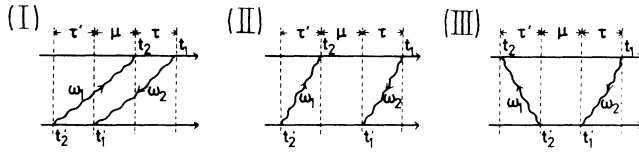


FIG. 1. Three typical diagrams are drawn according to the chronological order among four time variables t_1 , t_2 , t'_1 , and t'_2 . The time proceeds from left to right and the latest time is t_1 . The wavy lines represent the photon absorption and emission processes.

tribution from the successive terms in (2.15) cannot be neglected and the factorization approximation becomes invalid. Particularly for the term A_1 in (2.7), the contribution from a nonzero n gives rise to a broad Lorentzian-shaped Raman component with a half width at half maximum (HWHM) of $n\gamma_m$. As will be seen later, this contribution affects also the luminescence spectrum through its negative tail since the term A_1 vanishes when integrated over the emission frequency. In Fig. 2 the modulation rate is varied to cover the typical range from the slow-modulation regime to the fast-modulation regime while the modulation amplitude and the longitudinal relaxation rates of both the intermediate and final states are fixed. The incident light energy is chosen in the higher-energy side of the resonance. The emission spectrum calculated by the partial sum of the series in (2.15) up to the N th term will be denoted by S_N . Thus S_1 corresponds to the result of the factorization approximation. In the fast-modulation regime (c) the convergence of the successive terms in (2.15) is very rapid and S_2 gives almost S_∞ as the final result. In this case the factorization approxima-

tion gives a reasonable result. In the intermediate modulation regime (b), the convergence is not so fast and summation up to the fifth term is necessary to obtain a final result of S_∞ . In the slow-modulation regime (a) the partial sum up to at least the fifteenth term is required to get the final emission spectrum S_∞ . It is to be noted that S_2 gives a negative emission spectrum on the low-energy side. S_1 has a luminescence peak at $\Delta\omega_2=0$, whereas S_∞ ($\cong S_{15}$) does not have a luminescence peak but does have one peak at the energy of Raman scattering. The negative contribution from the broad Raman component erased the luminescence peak. Thus, the factorization approximation gives an erroneous result in the slow-modulation regime.

III. INTEGRATED INTENSITY OF RAMAN SCATTERING AND LUMINESCENCE AND THEIR EXCITATION SPECTRA

Experimentally the excitation spectra for the Raman scattering and the luminescence were obtained by measuring the integrated intensity of each component as a function of the off-resonance energy of the incident light. Here the integrated intensities of the Raman scattering and the luminescence are calculated theoretically and their excitation profiles are studied from the slow-modulation regime to the fast-modulation regime. The Raman component is identified with a sharp peak around $\Delta\omega_2=\Delta\omega_1$ after subtracting the broad background, namely, omitting the broad Raman component. On the other hand, the integrated intensity of the luminescence component is obtained by integrating the whole emission spectrum except the sharp Raman peak. This classification does not have a definite physical basis but corresponds to the actual procedure dealing with the experimental data.¹ The integrat-

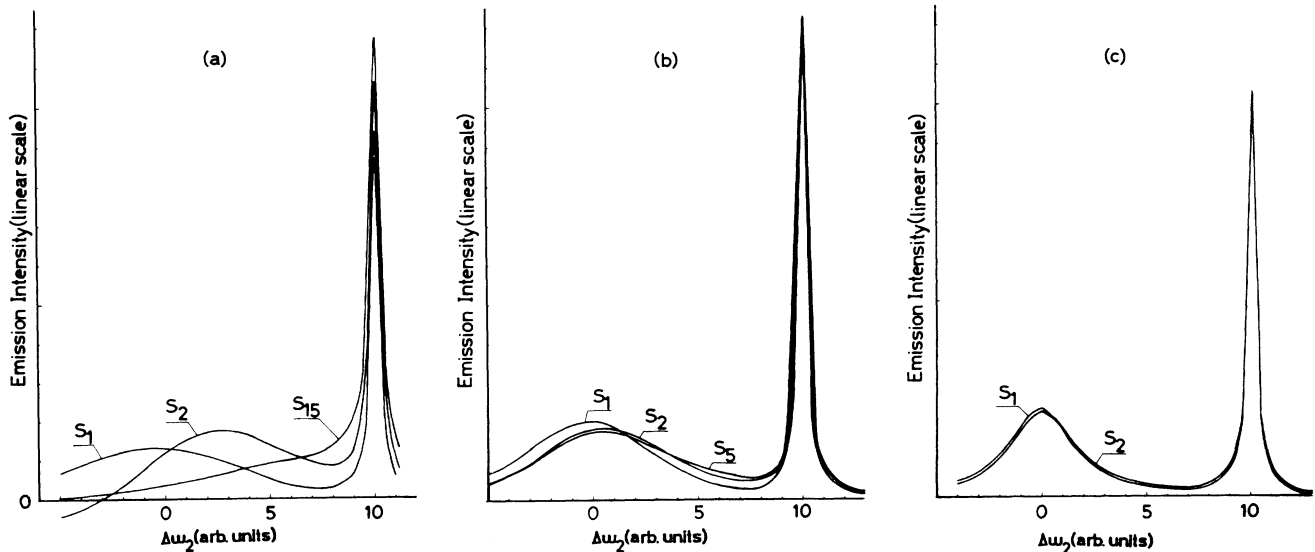


FIG. 2. Secondary emission spectra $I(\Delta\omega_1, \Delta\omega_2)$ are given as a function of the emission frequency $\Delta\omega_2$ for $\Delta\omega_1=10$ from the slow-modulation regime to the fast-modulation regime. The rates of the frequency modulation γ_m are (a) 0.4, (b) 4, and (c) 15, while the modulation amplitude Δ_m is fixed at 4, and half of the longitudinal relaxation rates are chosen as $\gamma_b=0.5$ and $\gamma_c=0.25$. The emission spectrum calculated by the partial sum of (2.15) up to the N th term is denoted by S_N . In each figure the final emission spectrum S_∞ is represented by S_N for the maximum number of N .

ed intensities of the Raman scattering and the luminescence will be denoted by $R(\Delta\omega)$ and $L(\Delta\omega)$, respectively, where $\Delta\omega$ is the off-resonance energy of the excitation light. The excitation spectra are obtained by normalizing $R(\Delta\omega)$ and $L(\Delta\omega)$ by the values $R(0)$ and $L(0)$, respectively. The excitation spectra are given in Fig. 3, where the parameter values are chosen as $\gamma_b=0.005$, $\gamma_c=0.0025$, $\Delta_m=1$, and γ_m is varied as 0.1, 1, and 10. The excitation light energy is chosen in the lower-energy side of the resonance. In the calculation the normalizing denominators $R(0)$ and $L(0)$ are replaced by the values of $R(\Delta\omega=-2)$ and $L(\Delta\omega=-2)$, respectively. In the intermediate- and the slow-modulation regimes, the excitation spectrum of the luminescence decreases faster than that of the Raman scattering and a substantial deviation appears between the two excitation profiles. This fast decrease in the luminescence intensity can be understood qualitatively as follows. The luminescence is the emission after the photoabsorption followed by relaxation and its intensity is proportional to the amount of dephasing that the excited level suffers during the period on the order of $|\Delta\omega|^{-1}$ where $\Delta\omega$ is the off-resonance energy of the excitation light. On the other hand, the total intensity of the secondary emission is determined by the photoabsorption process and is proportional to $(\Delta\omega)^{-2}$ in the large off-resonance region. Thus, roughly speaking, in the case of large off resonance the intensity of luminescence decreases more rapidly than that of Raman scattering by at least the factor $\gamma_m/|\Delta\omega|$. In the fast-modulation regime ($\gamma_m=10$) the excitation profile of the luminescence approaches that of the Raman scattering and shows the asymptotic behavior of $(\Delta\omega)^{-2}$ in the large off-resonance

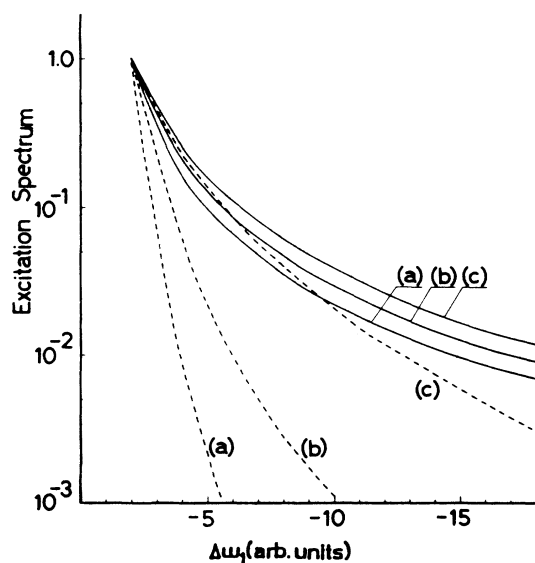


FIG. 3. Excitation profiles of the Raman scattering (solid line) and the luminescence (dashed line) are plotted without taking account of the inhomogeneous broadening. The rates of the frequency modulation γ_m are (a) 0.1, (b) 1, and (c) 10, while the modulation amplitude Δ_m is taken to be unity and half of the longitudinal relaxation rates are chosen as $\gamma_b=0.005$ and $\gamma_c=0.0025$.

region. These characteristic features of the excitation spectra can be useful in identifying which regime the system in question belongs to.

Besides the excitation spectra, the relative intensity ratio between the Raman scattering and the luminescence gives important information about the relaxation processes. Consider a quantity defined by

$$S(\Delta\omega) = \frac{L(\Delta\omega)}{R(\Delta\omega) + L(\Delta\omega)}. \quad (3.1)$$

This quantity is plotted in Fig. 4 using the same parameters as in Fig. 3. The quantity is quite sensitive to the parameter ratio Δ_m/γ_m . Thus, combining the excitation spectra and the plot of $S(\Delta\omega)$, the modulation parameters Δ_m and γ_m can be determined rather precisely.

Next, the effect of inhomogeneous broadening on the excitation spectra will be discussed. Inhomogeneous broadening is caused by several mechanisms. In the case of β -carotene in solutions, the effect of the thermal motion of the nearby solvent molecules on the energy levels of the β -carotene molecule can be decomposed into a random part with a time average of zero and a time-independent part that may be regarded as almost static during the light scattering process. The former part can be taken into account in terms of the random frequency modulation described in Sec. II, while the latter part can be attributed to inhomogeneous broadening.¹ The gross features of the excitation profiles are not changed by the inclusion of the inhomogeneous distribution of the intermediate-state energy. However, in order to determine the modulation parameters from the comparison between the experiment and the theory, the inhomogeneous distri-

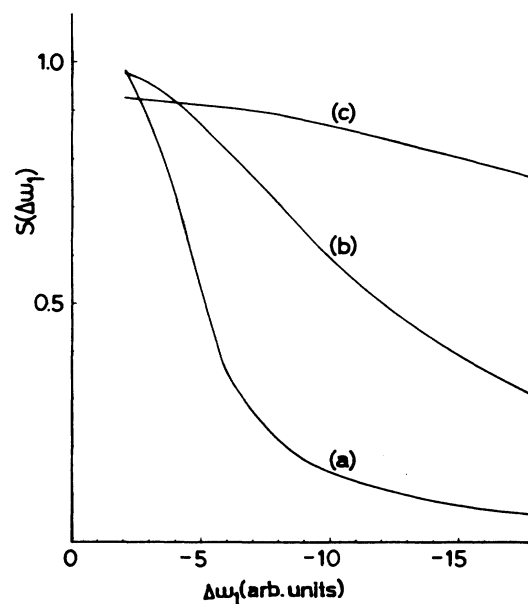


FIG. 4. The ratio $S(\Delta\omega_1)$ of the luminescence component to the total intensity is plotted as a function of the off-resonance energy $\Delta\omega_1$ of the incident light. The same parameter values as in Fig. 3 are chosen. The inhomogeneous broadening is not taken into account.

bution of the transition energy has to be taken into account. The inhomogeneous distribution of the intermediate-state energy can be assumed as Gaussian. The emission spectrum is calculated by

$$\int d\Delta E \exp\left[-\frac{(\Delta E)^2}{2\Delta_s^2}\right] I(\Delta\omega_1^0 - \Delta E, \Delta\omega_2^0 - \Delta E), \quad (3.2)$$

with $\Delta\omega_1^0 = \omega_1 - (E_b^0 - E_a)$, $\Delta\omega_2^0 = \omega_2 - (E_b^0 - E_c)$, and $\Delta E = E_b - E_b^0$ where I denotes the secondary emission spectrum calculated by (2.6) and E_b^0 and Δ_s are the peak energy and the standard deviation of the inhomogeneous distribution, respectively. Typical excitation spectra are shown in Fig. 5 for the intermediate-modulation regime, i.e., $\gamma_m = \Delta_m$ by assigning Δ_s the values Δ_m , $3\Delta_m$, and $5\Delta_m$. The absolute values of $R(\Delta\omega)/R(0)$ and $L(\Delta\omega)/L(0)$ depend sensitively on the inhomogeneous width. The excitation spectrum of the luminescence shows a Gaussian-type decrease as a function of the off-resonance energy, as seen clearly in the cases of $\Delta_s = 3\Delta_m$ and $5\Delta_m$. This behavior was actually observed in the experiments.¹ The effect of inhomogeneous broadening on the quantity $S(\Delta\omega)$ in (3.1) is also examined for the case of $\gamma_m = 1$ and $\Delta_m = 1$ by assigning the inhomogeneous width Δ_s the values Δ_m , $3\Delta_m$, and $5\Delta_m$. The results are shown in Fig. 6. The dependence on Δ_s is remarkable and this dependence can be useful in determining the modulation parameters γ_m and Δ_m and the inhomogeneous width Δ_s . As a consequence, it is important to take into account

the inhomogeneous distribution of the transition energy in order to estimate the modulation parameters and the inhomogeneous width from the experimental data. In fact, Watanabe *et al.*¹ estimated these parameters in the system of β -carotene in solutions by comparing the theoretical and experimental excitation profiles of the Raman scattering and the luminescence.

IV. TRANSIENT RESPONSE OF RAMAN SCATTERING AND LUMINESCENCE

The study of transient response under pulsed excitation is important in clarifying the dynamics and the relaxation processes in a material system. The transient secondary emission process was theoretically formulated first by Takagahara, Hanamura, and Kubo¹⁰ and the formulation was later improved by Hanamura and Takagahara.¹¹ The time-resolved emission spectra from a three-level system^{6,10} and from a localized electron-phonon system^{5,6,12,13} were studied extensively. The following clarifies the effect of the finite correlation time of frequency modulation on the transient behaviors of Raman scattering and luminescence.

According to the formulation by Hanamura and Takagahara,¹¹ the time-resolved emission spectrum at frequency ω_2 is calculated by the formula

$$I(\omega_1, \omega_2; T) = (\Delta T)^{-1} \sum_{\omega_2} |\Delta\psi^{(2)}(T)|^2, \quad (4.1)$$

with

$$\Delta\psi^{(2)}(T) = \int_T^{T+\Delta T} dt_1 \int_{-\infty}^{t_1} dt_2 \epsilon(t_2) e^{-i\omega_1 t_2 + i\omega_2 t_1} \langle c | e^{-iH(T-t_1)} V_{cb} e^{-iH(t_1-t_2)} V_{ba} e^{-iHt_2} | a \rangle, \quad (4.2)$$

where ω_1 and $\epsilon(t)$ are the carrier frequency and the envelope of the excitation pulse, respectively, $(T, T + \Delta T)$ is the time interval during which the photodetector is open, and the summation with respect to ω_2 is over the spectral width of the photodetector. The frequency-time uncertainty due to the finite observation period ΔT is incorporated automatically in terms of the finite interval integration with respect to t_1 , where t_1 implies the photon-emission time. Consequently, according to the diagrams in Fig. 1, the result is given by

$$I(\omega_1, \omega_2; T) = \text{Re}[B_I + B_{II} + B_{III}], \quad (4.3)$$

with

$$\begin{aligned} B_I &= \int_T^{T+\Delta T} dt_1 \int_T^{t_1} dt_2 \int_T^{t_2} dt'_1 \int_{-\infty}^{t'_1} dt'_2 \epsilon(t_2) \epsilon(t'_2) C(t_1 - t'_1) \\ &\quad \times \exp\{-(\gamma_b + \gamma_c - i\Delta\omega_2)(t_1 - t_2) - (\gamma_b + i\Delta\omega_1)(t'_1 - t'_2) \\ &\quad - [\gamma_c + i(\Delta\omega_1 - \Delta\omega_2)](t_2 - t'_1) - f_-(t_1 - t_2, t'_1 - t'_2, t_2 - t'_1)\} \\ &= \int_0^{\Delta T} d\tau \int_0^{\Delta T - \tau} d\mu \int_0^{\Delta T - \mu - \tau} dt'_1 \int_0^\infty d\tau' \epsilon(T + \mu + t'_1) \epsilon(T + t'_1 - \tau') C(\mu + \tau) \\ &\quad \times \exp\{-(\gamma_b + \gamma_c - i\Delta\omega_2)\tau - (\gamma_b + i\Delta\omega_1)\tau' \\ &\quad - [\gamma_c + i(\Delta\omega_1 - \Delta\omega_2)]\mu - f_-(\tau, \tau', \mu)\}, \end{aligned} \quad (4.4)$$

$$\begin{aligned} B_{II} &= \int_T^{T+\Delta T} dt_1 \int_T^{t_1} dt'_1 \int_{-\infty}^{t'_1} dt_2 \int_{-\infty}^{t_2} dt'_2 \epsilon(t_2) \epsilon(t'_2) C(t_1 - t'_1) \\ &\quad \times \exp[-(\gamma_b + \gamma_c - i\Delta\omega_2)(t_1 - t'_1) - (\gamma_b + i\Delta\omega_1)(t_2 - t'_2) \\ &\quad - 2\gamma_b(t'_1 - t_2) - f_-(t_1 - t'_1, t_2 - t'_2, t'_1 - t_2)] \end{aligned}$$

$$= \int_0^{\Delta T} d\tau \int_0^{\Delta T - \tau} dt'_1 \int_0^\infty d\mu \int_0^\infty d\tau' \epsilon(T + t'_1 - \mu) \epsilon(T + t'_1 - \mu - \tau') C(\tau) \times \exp[-(\gamma_b + \gamma_c - i\Delta\omega_2)\tau - (\gamma_b + i\Delta\omega_1)\tau' - 2\gamma_b\mu - f_-(\tau, \tau', \mu)] , \tag{4.5}$$

and

$$B_{III} = \int_T^{T+\Delta T} dt_1 \int_T^{t_1} dt'_1 \int_{-\infty}^{t'_1} dt'_2 \int_{-\infty}^{t'_2} dt_2 \epsilon(t_2) \epsilon(t'_2) C(t_1 - t'_1) \times \exp[-(\gamma_b + \gamma_c - i\Delta\omega_2)(t_1 - t'_1) - (\gamma_b - i\Delta\omega_1)(t'_2 - t_2) - 2\gamma_b(t'_1 - t'_2) - f_+(t_1 - t'_1, t'_2 - t_2, t'_1 - t'_2)] = \int_0^{\Delta T} d\tau \int_0^{\Delta T - \tau} dt'_1 \int_0^\infty d\mu \int_0^\infty d\tau' \epsilon(T + t'_1 - \mu - \tau') \epsilon(T + t'_1 - \mu) C(\tau) \times \exp[-(\gamma_b + \gamma_c - i\Delta\omega_2)\tau - (\gamma_b - i\Delta\omega_1)\tau' - 2\gamma_b\mu - f_+(\tau, \tau', \mu)] , \tag{4.6}$$

where the variable t'_1 is shifted by the amount T on the second line of each expression. The function $C(t)$ is the Fourier transform of the spectral resolution function $D(\omega)$ of the photodetector, namely,

$$C(t) = \int d\omega_2 D(\omega_2) e^{i(\omega_2 - \bar{\omega}_2)t} , \tag{4.7}$$

where $\bar{\omega}_2$ is the center frequency of $D(\omega)$. In the following $D(\omega)$ will be assumed as Lorentzian with a HWHM of γ_0 for simplicity. Hence $C(t)$ takes an exponential form as

$$C(t) \propto \exp(-\gamma_0 t) . \tag{4.8}$$

The pulse envelope will be taken in a realistic form, e.g., Gaussian form, and thus a Laplace transform is not convenient for carrying out the multifold integrations involving the pulse envelope $\epsilon(t)$. Instead, the Fourier

transform will be introduced as

$$\epsilon(t) = \int_{-\infty}^\infty d\omega f(\omega) e^{i\omega t} . \tag{4.9}$$

When the incident pulse envelope is Gaussian, i.e.,

$$\epsilon(t) = \frac{1}{\sqrt{2\pi}t_p} \exp\left[-\frac{t^2}{2t_p^2}\right] , \tag{4.10}$$

the associated spectral function $f(\omega)$ is given by

$$f(\omega) = (2\pi)^{-1} \exp(-\omega^2 t_p^2 / 2) , \tag{4.11}$$

where t_p is the standard deviation of the pulse width.

By introducing the scaling defined by (2.13) and making use of the expansion in (2.15), each contribution of B_I , B_{II} , and B_{III} in (4.4)–(4.6) can be rewritten in a tractable form as

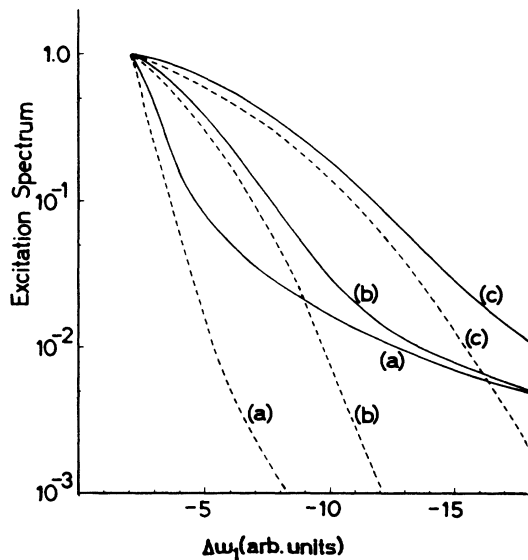


FIG. 5. Excitation profiles of the Raman scattering (solid line) and the luminescence (dashed line) are plotted taking into account the inhomogeneous broadening. The inhomogeneous width Δ_s is varied at the values (a) Δ_m , (b) $3\Delta_m$, and (c) $5\Delta_m$, while the modulation amplitude and rate are fixed as $\Delta_m = 1$ and $\gamma_m = 1$, respectively, and half of the longitudinal relaxation rates are chosen as $\gamma_b = 0.005$ and $\gamma_c = 0.0025$.

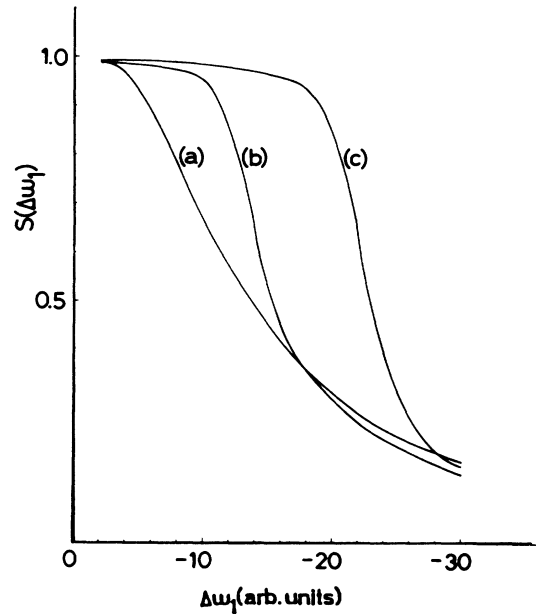


FIG. 6. The ratio $S(\Delta\omega_1)$ of the luminescence component to the total intensity is plotted as a function of the off-resonance energy $\Delta\omega_1$ of the incident light taking into account the inhomogeneous broadening. The same parameter values are chosen as in Fig. 5.

$$\begin{aligned}
B_I = & \int d\omega \int d\omega' \frac{f(\omega)f(\omega')}{i(\omega+\omega')} e^{i(\omega+\omega')T} \\
& \times \sum_{n=0}^{\infty} (n!)^{-1} \int_0^{\Delta_m \Delta T} du \int_0^{\infty} du' [ug(u)]^n [u'g(u')]^n \\
& \times \exp[-\bar{\sigma}u - (\bar{\sigma}' + \xi')u' - a(e^{-pu} + pu - 1) - a(e^{-pu'} + pu' - 1)] \\
& \times [e^{i(\omega+\omega')\Delta T} (e^{-\xi_1 u} - e^{-\xi_1 \Delta T - (\xi_1 - \xi_1/\Delta_m)u}) / \xi_1 \\
& - (e^{-\xi_2 u} - e^{-\xi_2 \Delta T - (\xi_2 - \xi_2/\Delta_m)u}) / \xi_2], \tag{4.12}
\end{aligned}$$

with

$$\begin{aligned}
\xi_1 = & [\gamma_0 + i(\omega + \omega')] / \Delta_m, \quad \xi_2 = \gamma_0 / \Delta_m, \quad \xi_1 = n\gamma_m + \gamma_0 + z + i\omega', \\
\xi_2 = & n\gamma_m + \gamma_0 + z - i\omega, \quad \xi' = i\omega' / \Delta_m, \quad z = \gamma_c + i(\Delta\omega_1 - \Delta\omega_2), \\
\bar{\sigma} = & (\gamma_b + \gamma_c - i\Delta\omega_2) / \Delta_m, \quad \bar{\sigma}' = (\gamma_b + i\Delta\omega_1) / \Delta_m, \tag{4.13}
\end{aligned}$$

$$\begin{aligned}
B_{II} = & \int d\omega \int d\omega' \frac{f(\omega)f(\omega')}{i(\omega+\omega')} e^{i(\omega+\omega')T} \\
& \times \sum_{n=0}^{\infty} (n!)^{-1} \frac{1}{n\gamma_m + z + i(\omega + \omega')} \\
& \times \int_0^{\Delta_m \Delta T} du \int_0^{\infty} du' [ug(u)]^n [u'g(u')]^n (e^{i(\omega+\omega')\Delta T - \xi_1 u} - e^{-\xi_2 u}) \\
& \times \exp[-\bar{\sigma}u - (\bar{\sigma}' + \xi')u' - a(e^{-pu} + pu - 1) - a(e^{-pu'} + pu' - 1)], \tag{4.14}
\end{aligned}$$

with

$$\bar{\sigma} = (\gamma_b + \gamma_c - i\Delta\omega_2) / \Delta_m, \quad \bar{\sigma}' = (\gamma_b - i\Delta\omega_1) / \Delta_m, \quad z = 2\gamma_b, \tag{4.15}$$

and

$$\begin{aligned}
B_{III} = & \int d\omega \int d\omega' \frac{f(\omega)f(\omega')}{i(\omega+\omega')} e^{i(\omega+\omega')T} \\
& \times \sum_{n=0}^{\infty} \frac{(-1)^n}{n!} \frac{1}{n\gamma_m + z + i(\omega + \omega')} \\
& \times \int_0^{\Delta_m \Delta T} du \int_0^{\infty} du' [ug(u)]^n [u'g(u')]^n (e^{i(\omega+\omega')\Delta T - \xi_1 u} - e^{-\xi_2 u}) \\
& \times \exp[-\bar{\sigma}u - (\bar{\sigma}' + \xi')u' - a(e^{-pu} + pu - 1) - a(e^{-pu'} + pu' - 1)], \tag{4.16}
\end{aligned}$$

with

$$\begin{aligned}
\bar{\sigma} = & (\gamma_b + \gamma_c - i\Delta\omega_2) / \Delta_m, \\
\bar{\sigma}' = & (\gamma_b + i\Delta\omega_1) / \Delta_m, \\
z = & 2\gamma_b, \tag{4.17}
\end{aligned}$$

where ξ_1 , ξ_2 , and ξ' are common to the three terms. The integrations with respect to u and u' are decoupled and can be easily carried out. The u' integral over a semi-infinite interval can be calculated by the formalism given in Appendix A and the u integral over a finite interval can be performed directly or by the inhomogeneous continued fraction representation developed in Appendix B.

Typical transient responses of the Raman scattering

and the luminescence are shown in Figs. 7–12. In the calculation, the center frequency $\bar{\omega}_2$ in (4.7) is set either at the Raman line or at the luminescence line. The relevant parameters are chosen as

$$\begin{aligned}
\Delta_m = & 1, \quad \gamma_b = 0.005, \quad \gamma_c = 0.0025, \\
\gamma_0 = & 0.5, \quad t_p = 20, \quad \Delta T = 5,
\end{aligned}$$

the modulation rate γ_m is assigned the values 0.1, 1, and 10, and the off-resonance energies of the incident light $\Delta\omega_1$ are chosen as -15 , -10 , and -5 . The unit of time is taken to be the inverse of the unit of energy (frequency). The calculated intensity is normalized so that the maximum value is unity. The maximum point of the Raman

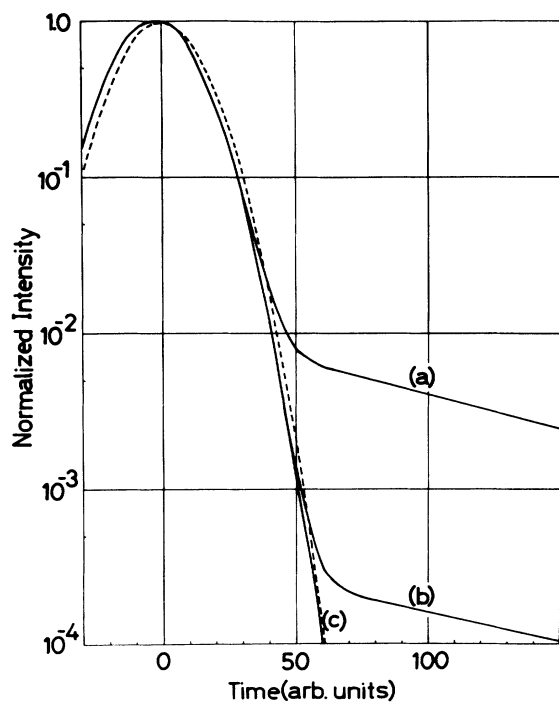


FIG. 7. Transient behavior of the emission intensity at the Raman line. The envelope of the excitation pulse intensity is given by the dashed curve. The off-resonance energy of the incident light $\Delta\omega_1$ is varied at the values (a) -5 , (b) -10 , and (c) -15 , while the modulation amplitude and modulation rate are taken as $\Delta_m=1$ and $\gamma_m=0.1$, respectively, and half of the longitudinal relaxation rates are chosen as $\gamma_b=0.005$ and $\gamma_c=0.0025$. The pulse width t_p (standard deviation) is 20 and the spectral resolution γ_0 and the time gate width ΔT of the photodetector are 0.5 and 5, respectively.

component is almost coincident with the incident pulse peak, while that of the luminescence component is considerably delayed from the pulse peak. In general the Raman component responds quickly to the excitation pulse and its transient behavior is very close to the envelope of the excitation pulse intensity. In the long-time tail of the transient response there appears a slow component reminiscent of luminescence. This mixing of the luminescence component into the Raman component is due to the spectral resolution function $D(\omega)$ in (4.7) that covers the luminescence line in the Lorentzian tail, and is also due to the broad background of luminescence that is present even at the Raman frequency. The intensity of the slow component decreases quickly as the off-resonance energy $|\Delta\omega_1|$ increases, as can be seen from Figs. 7–9. The slow component decreases most rapidly in the slow-modulation regime when the off-resonance energy $|\Delta\omega_1|$ is increasing. This corresponds to the fact that the excitation spectrum of the luminescence decreases most rapidly in the slow-modulation regime as a function of the off-resonance energy.

On the other hand, the transient response of the luminescence line is quite different from that of the Ra-

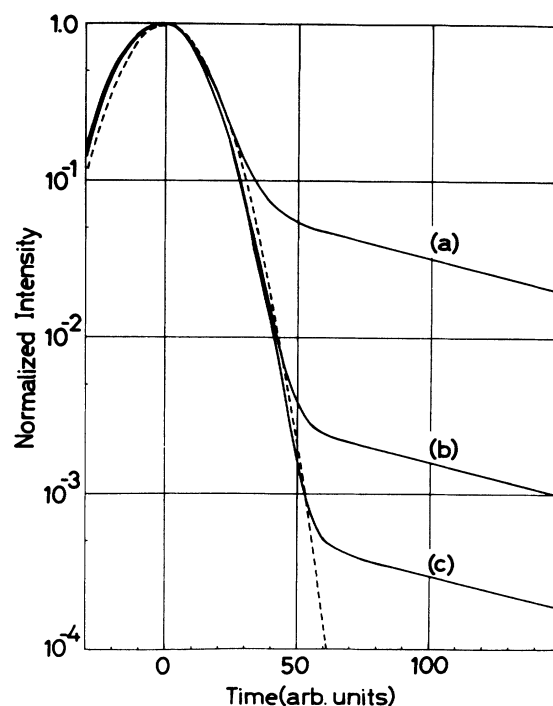


FIG. 8. Transient behavior of the emission intensity at the Raman line. The parameters are the same as in Fig. 7 except that the modulation rate γ_m is 1.

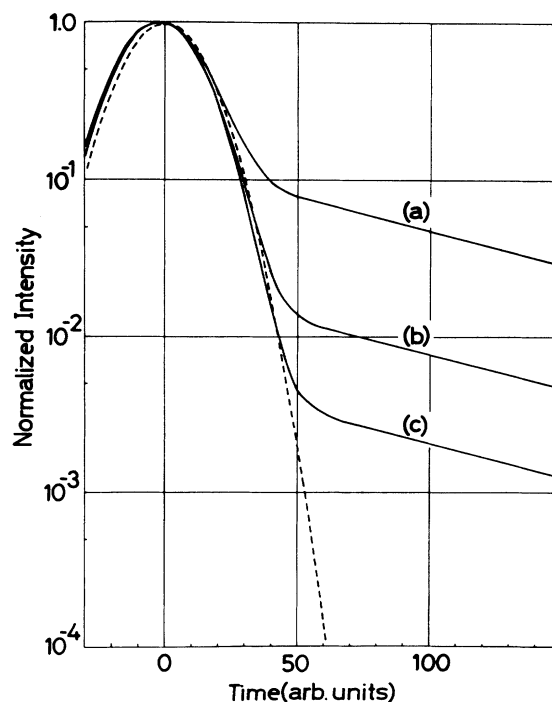


FIG. 9. Transient behavior of the emission intensity at the Raman line. The parameters are the same as in Fig. 7 except that the modulation rate γ_m is 10.

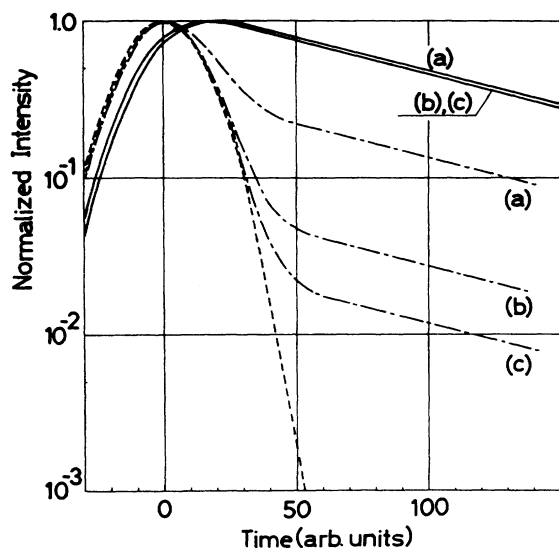


FIG. 10. Transient behavior of the emission intensity at the luminescence line (solid curve) and the population of the intermediate state (dot-dashed curve). The off-resonance energy $\Delta\omega_1$ of the incident light is varied at the values (a) -5 , (b) -10 , and (c) -15 . The intensity envelope of the excitation pulse is given by the dashed curve. The modulation amplitude and modulation rate are chosen as $\Delta_m=1$ and $\gamma_m=0.1$, respectively. The other parameters are the same as in Fig. 7.

man line. First, the temporal peak of the luminescence component is delayed from that of the incident pulse envelope. Second, the decay characteristics are determined by the longitudinal relaxation constant of the intermediate

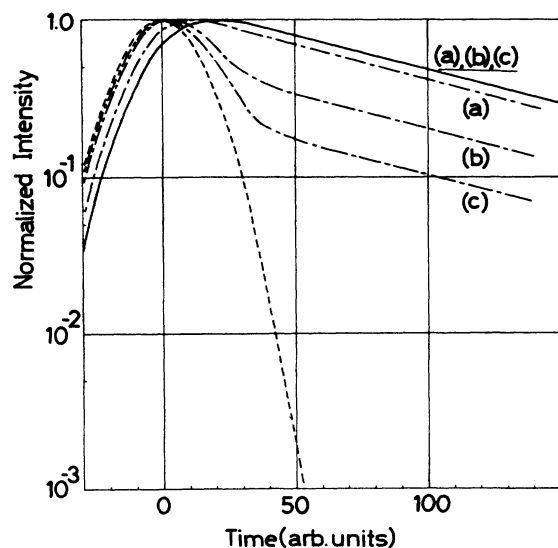


FIG. 11. Transient behavior of the emission intensity at the luminescence line (solid curve) and the population of the intermediate state (dot-dashed curve). The same parameter values are chosen as in Fig. 10 except that the modulation rate γ_m is 1. The curves (a), (b), and (c) of the luminescence intensity almost overlap.

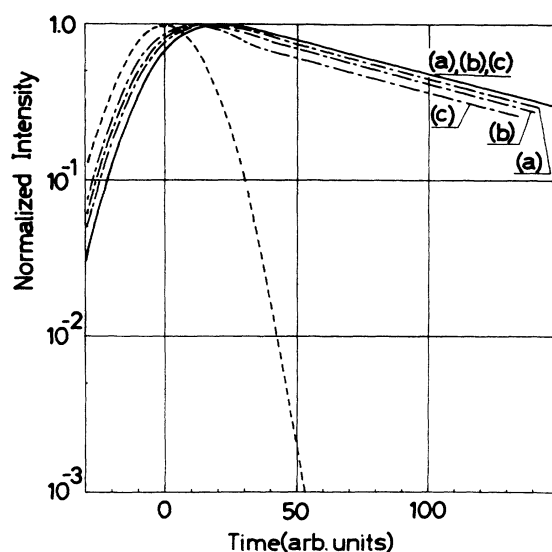


FIG. 12. Transient behavior of the emission intensity at the luminescence line (solid curve) and the population of the intermediate state (dot-dashed curve). The same parameter values are chosen as in Fig. 10 except that the modulation rate γ_m is 10. The curves (a), (b), and (c) of the luminescence intensity almost overlap.

(excited) state and are almost independent of the off-resonance energy and also of the modulation rate. It is interesting to compare the transient behavior of the luminescence intensity with that of the intermediate-state population since the luminescence intensity is usually considered to be proportional to the latter. The intermediate-state population $P_b(t)$ under pulsed excitation is given by, apart from unimportant factors,

$$P_b(t) = \text{Re} \left[\int d\omega \int d\omega' f(\omega) f(\omega') \frac{e^{i(\omega+\omega')t}}{2\gamma_b + i(\omega+\omega')} \right. \\ \left. \times I_0 \left[\frac{\gamma_b + i(\omega' + \Delta\omega_1)}{\Delta_m} \right] \right], \quad (4.18)$$

where the notations are the same as in (4.12)–(4.17) and I_0 is given in Appendix A. The calculated results are shown in Figs. 10–12 by dot-dashed curves which are normalized such that the maximum value is unity. Unexpectedly enough, a large difference is found between the luminescence intensity and $P_b(t)$ especially in the case of the intermediate- and slow-modulation regimes. In these regimes it can be considered that the coherent interaction with the radiation field is dominant during the pulse excitation and the intermediate state is excited adiabatically. Thus $P_b(t)$ follows the intensity envelope of the excitation pulse at the initial stage. After the coherence of excitation faded out, $P_b(t)$ decays with the radiative lifetime. These features are more remarkable for larger off-resonances $|\Delta\omega_1|$. Experimentally the intermediate-state population $P_b(t)$ can be monitored by the spectrally integrated emission intensity over the whole emission band.

In fact, it can be shown that

$$\int d\omega_2 I(\omega_1, \omega_2; T) \propto (\Delta T)^{-1} \int_T^{T+\Delta T} dt P_b(t). \quad (4.19)$$

The experimental observation of the above difference is quite interesting to reveal the effect of the finite correlation time of frequency modulation.

The calculated transient response $I_R(t)$ at the Raman frequency can be fitted by a linear combination of the Gaussian pulse shape and the convoluted pulse shape with the longitudinal decay curve, namely,

$$I_R(t) = A_F \exp(t/t_p)^2 + A_S \int_{-\infty}^t dt' e^{-2\gamma_b(t-t')} \exp(t'/t_p)^2. \quad (4.20)$$

The first and second terms in (4.20) can be interpreted as the fast component and the slow component, respectively. Accordingly, the time-integrated intensities of these components are given by

$$I_F = \sqrt{\pi} t_p A_F, \quad I_S = \sqrt{\pi} t_p A_S / (2\gamma_b), \quad (4.21)$$

respectively, where the subscript F (S) refers to the fast (slow) component. The ratio of the intensity of the slow component to the total intensity is defined by the expression

$$R = I_S / (I_S + I_F) \quad (4.22)$$

and will be examined as a function of the off-resonance energy $\Delta\omega_1$. The results are plotted in Fig. 13. Although only a few points are calculated, the general trend can be clearly seen. The ratio R shows the steepest decrease in the slow-modulation regime as the off-resonance energy increases. This type of figure can be useful in determining the modulation parameters from the experimental data. It is important to note that the ratio R of (4.22) is quite different from the ratio $S(\Delta\omega)$ in (3.1) which is associated with the spectrally integrated intensity. This is because the time-integrated intensity in (4.21) is spectrally limited by the spectral resolution function $D(\omega)$ in (4.7).

In addition the effect of the finite observation period ΔT on the time-resolved emission spectra should be mentioned. When ΔT is reduced, the emission spectrum becomes broader as a consequence of the frequency-time uncertainty. Moreover, when the observation period ΔT becomes shorter, the intensity ratio of the Raman component to the luminescence component decreases since the integration range of t_2 is limited by ΔT for the term B_1 which contributes to the Raman component. As a result, the ratio R of (4.22) becomes larger for shorter ΔT . This is confirmed by the comparison of Fig. 13 with Fig. 14 which shows R for the same parameters as in Fig. 13 except that $\Delta T = 0.5$. Thus the details of the observation conditions, e.g., $D(\omega)$ and the observation period ΔT must be specified carefully in the analysis of experimental data to determine the modulation parameters.

Mukamel *et al.*¹⁴ identified the slow component by another criterion for a particular shape of the excitation pulse and discussed the dependence of a quantity similar to (4.22) on the off-resonance energy. However, in their work only the total intensity of the secondary emission is concerned and spectral resolution is not attempted. Thus

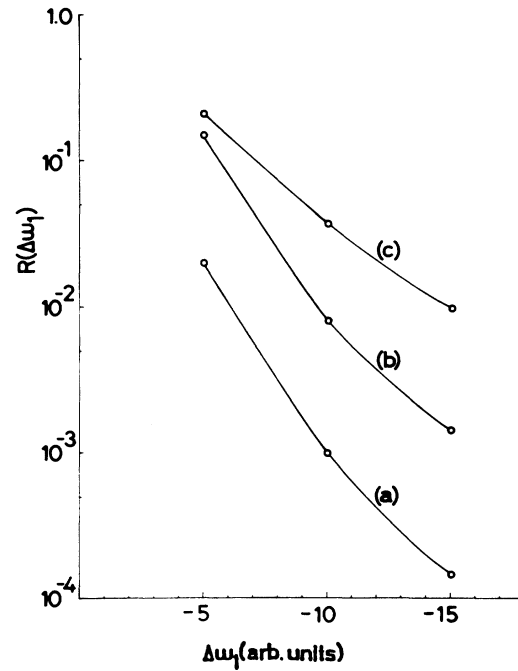


FIG. 13. The ratio R of the slow component to the total intensity is calculated from the transient response curves at the Raman line in Figs. 7–9, according to formulas (4.21) and (4.22). The solid curves are drawn only to guide the eye. The modulation rate γ_m is varied at the values (a) 0.1, (b) 1, and (c) 10, while the modulation amplitude Δ_m is fixed to be 1.

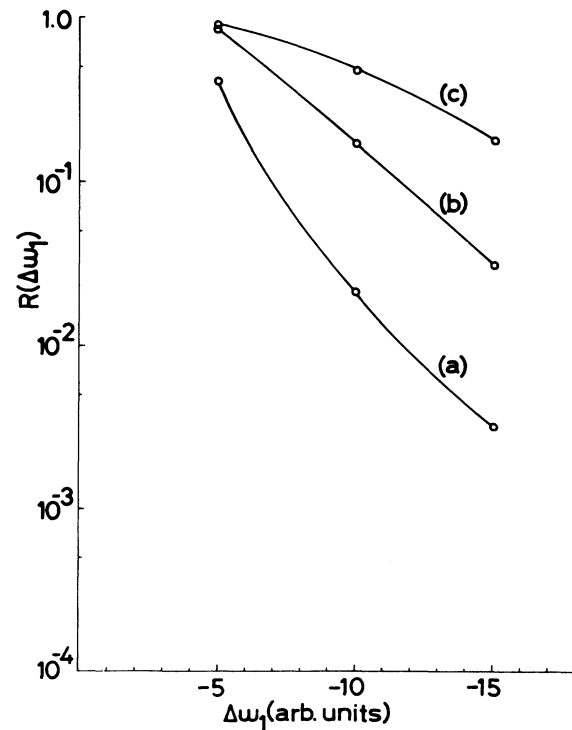


FIG. 14. The ratio R of the slow component to the total intensity at the Raman line. The parameters are the same as in Fig. 13 except that the observation period (time gate width) ΔT is 0.5. The solid curves are drawn only to guide the eye.

a comparison of our results with theirs is not relevant.

As seen above, the transient emission intensity at the Raman frequency has both the fast and slow components, whereas the slow component is predominant in the transient behavior of the emission intensity at the luminescence frequency. It is interesting to study the transient behavior of the emission intensity at the frequencies between the Raman line and the luminescence line. Typical results are given in Figs. 15–17 for the parameters

$$\Delta\omega_1 = -10, \quad \Delta_m = 1, \quad \gamma_b = 0.005, \quad \gamma_c = 0.0025,$$

and by varying the modulation rate γ_m , to be 0.1, 1, and 10. Four emission frequencies were selected between the Raman line and the luminescence line for $\Delta\omega_2 = -2, -4, -6,$ and -8 . The character of the transient behavior changes continuously from a Raman-like one to a luminescencelike one across the emission frequencies. This change of character can be estimated by the change in the quantity R defined by (4.22). The change in R as a function of the emission frequency is plotted in Fig. 18 for the three representative modulation regimes by fixing the off-resonance energy of the incident light $\Delta\omega_1$ and the modulation amplitude Δ_m . Although the number of calculated points is rather limited, the characteristic trend can be clearly seen. Around the luminescence frequency ($\Delta\omega_2 = 0$), the ratio of the slow component to the total intensity is nearly unity. This type of plot can also be useful in estimating the modulation parameters.

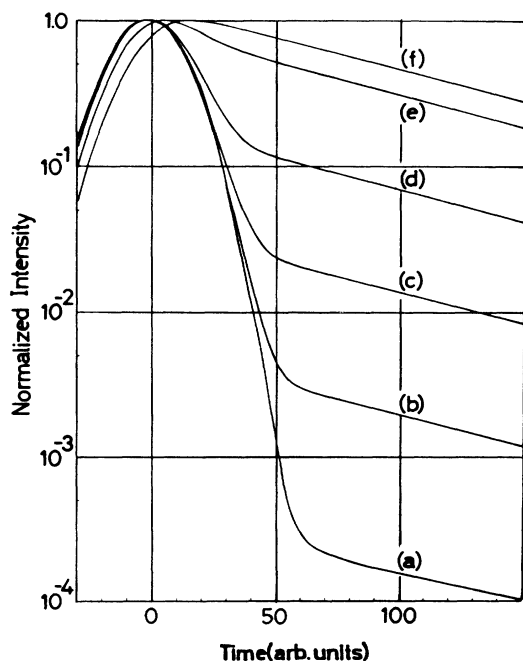


FIG. 15. Transient behavior of the emission intensity at several emission frequencies $\Delta\omega_2$ between the Raman line and the luminescence line, namely, (a) -10 , (b) -8 , (c) -6 , (d) -4 , (e) -2 , and (f) 0 , for the off-resonance energy of the incident light $\Delta\omega_1$ chosen as -10 . The amplitude and rate of the frequency modulation are chosen as $\Delta_m = 1$ and $\gamma_m = 0.1$, respectively. The other parameters are the same as in Fig. 7.

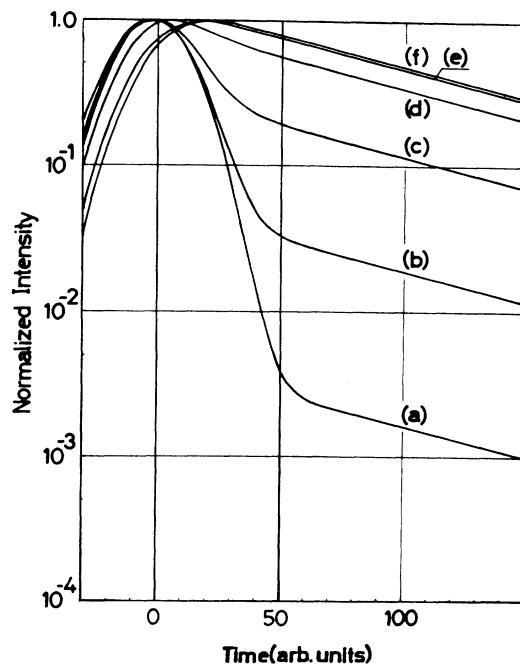


FIG. 16. Transient behavior of the emission intensity at several emission frequencies between the Raman line and the luminescence line. The notations and parameter values are the same as in Fig. 15 except that the modulation rate γ_m is 1.

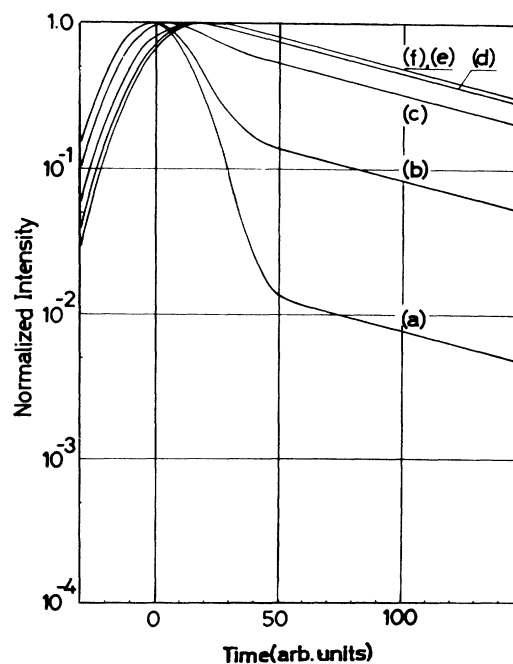


FIG. 17. Transient behavior of the emission intensity at several emission frequencies between the Raman line and the luminescence line. The notations and parameter values are the same as in Fig. 15 except that the modulation rate γ_m is 10.

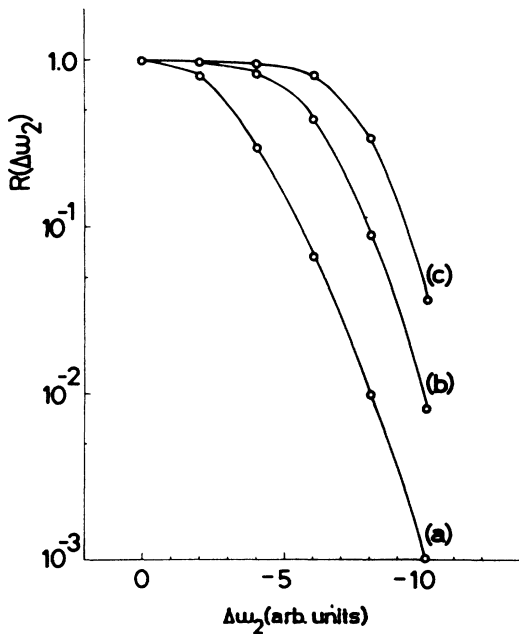


FIG. 18. The ratio R of the slow component to the total intensity is plotted as a function of the emission frequency $\Delta\omega_2$, while the off-resonance energy of the incident light $\Delta\omega_1$ is fixed to be -10 . The rate γ_m of the frequency modulation is varied at the values (a) 0.1, (b) 1, and (c) 10. The other parameters are the same as in Fig. 15. The solid curves are drawn only to guide the eye.

In final consideration, the study of the transient response of the Raman scattering and the luminescence under pulsed excitation is quite important to reveal the dynamics of the system in question and to determine the various relaxation parameters in combination with the spectral characteristics of the emission under stationary excitation. The longitudinal relaxation rate can be determined from the decay profile of the luminescence component, and the modulation parameters can be estimated from the dependence of the decay characteristics of the Raman component on the off-resonance energy of the excitation light and on the emission frequency.

V. SUMMARY

The effects of the finite correlation time of the frequency modulation or, in other words, the nonmotional narrowing effects on the secondary emission spectra have been clarified on the basis of the general stochastic theory. With respect to the emission spectra under stationary excitation, the luminescence component tends to be reduced relative to the Raman scattering component in the slow-modulation regime. The excitation spectrum of the luminescence decreases more rapidly than that of the Raman scattering as the off-resonance energy of the excitation light increases. This trend can be understood by noting that the period of staying in the excited state is inversely proportional to the off-resonance energy and that the luminescence component arises from the dephased

part of the excitation. In the transient response, the luminescence component decays exponentially with the longitudinal relaxation rate of the excited state. It is found for the first time that the difference is unexpectedly large between the transient behavior of the luminescence intensity and that of the intermediate-state population for the slow-modulation regime and that the difference can be an indicator of the nonmotional narrowing effect. The Raman component shows two kinds of transient behavior: one is a fast response following closely the excitation pulse envelope and the other is the same exponential decay as the luminescence component. The ratio of the slow component to the total intensity at the Raman line is sensitively dependent on the modulation parameters, i.e., the correlation time and the amplitude of modulation. The modulation parameters can be estimated from the experimental data by making use of these dependences.

The present theory has been applied successfully to interpret the experiments by Watanabe *et al.*¹ on the secondary emission spectra from β -carotene in solutions. Recently the nonmotional narrowing effect on the secondary emission spectra has been found in various kinds of materials. Nakamura *et al.*¹⁵ observed this effect in the LO-phonon Raman spectra from $\text{Cd}_x\text{Zn}_{1-x}\text{Te}$ mixed crystals and Kato *et al.*¹⁶ found the same effect in the vibronic Raman spectra from NaNO_2 crystals. These experimental data can be interpreted in terms of the present stochastic theory. However, in order to understand the microscopic mechanisms of the frequency modulation and to estimate the modulation parameters quantitatively, additional detailed studies are necessary on both the theoretical and experimental aspects.

ACKNOWLEDGMENTS

The author would like to thank Professor T. Kushida, Dr. S. Kinoshita, and Dr. J. Watanabe for enlightening discussions on their experimental data prior to publication. Thanks are also due to Professor R. Kubo and Professor E. Hanamura for continual encouragements and to Professor Y. Toyozawa for critical comments on the stochastic theory. A part of this work has been done at the Department of Applied Physics, the University of Tokyo under financial support from the Ministry of Education, Science and Culture of Japan.

APPENDIX A: HOMOGENEOUS CONTINUED-FRACTION REPRESENTATION

In this appendix we describe the continued-fraction representation of the integral given by

$$I_n(\sigma) = \int_0^\infty du [ug(u)]^n \exp[-\sigma u - a\phi(u)], \quad (\text{A1})$$

with

$$g(u) = \frac{1 - e^{-pu}}{pu}, \quad \phi(u) = e^{-pu} + pu - 1, \quad a = 1/p^2, \quad (\text{A2})$$

where σ is a complex number and p is a real constant. First, let us consider the following integrals:

$$J_n(\sigma) = \int_0^\infty du (1 - e^{-pu})^n \exp[-\sigma u - a\phi(u)] \quad (n = 0, 1, 2, \dots) \quad (A3)$$

Partially integrating (A3) and using the relations

$$\phi'(u) = p(1 - e^{-pu}) \text{ and } \phi''(u) = p[p - \phi'(u)], \quad (A4)$$

we find the recurrence relations

$$p^{-1}J_1(\sigma) = 1 - \sigma J_0(\sigma), \quad (A5)$$

and

$$p^{-1}J_{n+1}(\sigma) = npJ_{n-1}(\sigma) - (\sigma + np)J_n(\sigma) \quad (n \geq 1). \quad (A6)$$

Since $I_n(\sigma) = J_n(\sigma)/p^n$, the recurrence relations for $[I_n(\sigma)]_{n=0}^\infty$ are given by the equations

$$I_1(\sigma) = 1 - \sigma I_0(\sigma), \quad (A7)$$

and

$$I_{n+1}(\sigma) = nI_{n-1}(\sigma) - (\sigma + np)I_n(\sigma) \quad (n \geq 1). \quad (A8)$$

These recurrence equations are solved as follows:

$$\begin{aligned} I_0(\sigma) &= \frac{1}{1/I_0(\sigma)} = \frac{1}{\sigma + I_1(\sigma)/I_0(\sigma)} \\ &= \frac{1}{\sigma + \frac{1}{\sigma + p + I_2(\sigma)/I_1(\sigma)}} \\ &= \frac{1}{\sigma + \frac{1}{\sigma + p + \frac{2}{\sigma + 2p + \dots}}}, \end{aligned} \quad (A9)$$

and

$$I_n(\sigma) = \frac{nI_{n-1}(\sigma)}{\sigma + np + \frac{n+1}{\sigma + (n+1)p + \frac{n+2}{\sigma + (n+2)p + \dots}} \quad (n \geq 1). \quad (A10)$$

The foregoing results can be written more compactly through introducing the functions $[K_n(\sigma)]_{n=0}^\infty$ defined by

$$K_0(\sigma) = \sigma + \frac{1}{\sigma + p + \frac{2}{\sigma + 2p + \dots}}, \quad (A11)$$

and

$$K_n(\sigma) = \sigma + np + \frac{n+1}{\sigma + (n+1)p + \frac{n+2}{\sigma + (n+2)p + \dots}} \quad (n \geq 1). \quad (A12)$$

A recurrence relation exists such that

$$K_n(\sigma) = \sigma + np + \frac{n+1}{K_{n+1}(\sigma)} \quad (n \geq 0). \quad (A13)$$

Accordingly, Eqs. (A9) and (A10) can be rewritten as

$$I_0(\sigma) = \frac{1}{K_0(\sigma)}, \quad (A14)$$

and

$$I_n(\sigma) = \frac{n!}{K_n(\sigma)K_{n-1}(\sigma)\dots K_0(\sigma)} \quad (n \geq 1). \quad (A15)$$

The above continued-fraction representation is rapidly convergent over the entire range of the parameter p and is convenient for calculating numerically the integral in (A1).

APPENDIX B: INHOMOGENEOUS CONTINUED-FRACTION REPRESENTATION

The continued-fraction representation is presented for a finite-interval integral defined by

$$H_n(\sigma) = \int_0^M du [ug(u)]^n \exp[-\sigma u - a\phi(u)] \quad (n = 0, 1, 2, \dots), \quad (B1)$$

where the notations are the same as in Appendix A and M is the upper bound of the integral. In this case inhomogeneous terms appear in the recurrence relations due to finite interval integration; namely,

$$H_1(\sigma) = \beta_1 - \sigma H_0(\sigma), \quad (B2)$$

and

$$H_{n+1}(\sigma) = \beta_{n+1} - (\sigma + np)H_n(\sigma) + nH_{n-1}(\sigma) \quad (n \geq 1), \quad (B3)$$

where

$$\beta_1 = 1 - \exp[-\sigma M - a\phi(M)], \quad (B4)$$

and

$$\beta_{n+1} = -[(1 - e^{-pM})/p]^n \exp[-\sigma M - a\phi(M)] \quad (n \geq 1). \quad (B5)$$

Since the recurrence equations are linear with respect to $[H_j(\sigma)]_{j=0}^\infty$, the solution is given by the sum of solutions as

$$[H_j(\sigma)]_{j=0}^\infty = \sum_{n=1}^\infty [H_j^{(n)}(\sigma)]_{j=0}^\infty, \quad (B6)$$

where $[H_j^{(n)}(\sigma)]_{j=0}^\infty$ is the solution of the modified-recurrence equations in which only one inhomogeneous term β_n is retained. The modified-recurrence equations are given as

$$H_1(\sigma) = -\sigma H_0(\sigma), \quad (B7)$$

$$H_2(\sigma) = H_0(\sigma) - (\sigma + p)H_1(\sigma), \quad (B8)$$

\vdots

$$H_{n-1}(\sigma) = (n-2)H_{n-3}(\sigma) - [\sigma + (n-2)p]H_{n-2}(\sigma), \quad (B9)$$

$$H_n(\sigma) = \beta_n + (n-1)H_{n-2}(\sigma) - [\sigma + (n-1)p]H_{n-1}(\sigma), \quad (B10)$$

$$\begin{aligned} H_{n+1}(\sigma) &= nH_{n-1}(\sigma) - (\sigma + np)H_n(\sigma), \\ &\vdots \end{aligned} \quad (\text{B11})$$

For Eq. (B11) and the following, the solution is obtained in the same way as in Appendix A and is given by

$$H_n(\sigma) = nH_{n-1}(\sigma)/K_n(\sigma), \quad (\text{B12})$$

and

$$H_{n+1}(\sigma) = (n+1)H_n(\sigma)/K_{n+1}(\sigma), \quad (\text{B13})$$

and so on. Then, substitution of (B12) into (B10) leads to the equation

$$\begin{aligned} [\sigma + (n-1)p + n/K_n(\sigma)]H_{n-1}(\sigma) \\ = \beta_n + (n-1)H_{n-2}(\sigma). \end{aligned} \quad (\text{B14})$$

On account of the recurrence relation (A13) the factor within the parentheses on the left side of (B14) is equal to $K_{n-1}(\sigma)$. Hence we get

$$H_{n-1}(\sigma) = [\beta_n + (n-1)H_{n-2}(\sigma)]/K_{n-1}(\sigma), \quad (\text{B15})$$

and again substituting this relation into (B9) we find

$$H_{n-2}(\sigma) = \frac{(n-2)H_{n-3}(\sigma)}{K_{n-2}(\sigma)} - \frac{\beta_n}{K_{n-2}(\sigma)K_{n-1}(\sigma)}. \quad (\text{B16})$$

An $n-1$ times repetition of this procedure leads to the result

$$H_1(\sigma) = \frac{H_0(\sigma)}{K_1(\sigma)} + \frac{(-1)^n \beta_n}{K_1(\sigma)K_2(\sigma) \cdots K_{n-1}(\sigma)}. \quad (\text{B17})$$

Then, by combining (B17) with (B7), we obtain the expression

$$H_0(\sigma) = \frac{(-1)^{n+1} \beta_n}{K_0(\sigma)K_1(\sigma) \cdots K_{n-1}(\sigma)}. \quad (\text{B18})$$

$H_1(\sigma)$, $H_2(\sigma)$, . . . , and $H_{n-1}(\sigma)$ can be calculated successively by using the recurrence relations (B7)–(B9). Once $H_{n-1}(\sigma)$ is obtained, $H_n(\sigma)$ and the following can be calculated by the recurrence relations (B12) and (B13).

Then, taking the sum of the solutions thus obtained for each n , the solution of the inhomogeneous recurrence equations (B2) and (B3) can finally be obtained. This formalism converges quite rapidly and is more efficient than direct integration, especially for large values of M .

- ¹J. Watanabe, S. Kinoshita, and T. Kushida, Chem. Phys. Lett. **126**, 197 (1986); S. Kinoshita, J. Watanabe, and T. Kushida, J. Phys. (Paris) Colloq. **C7**, 419 (1985).
²T. Takagahara, E. Hanamura, and R. Kubo, J. Phys. Soc. Jpn. **43**, 802 (1977).
³T. Takagahara, E. Hanamura, and R. Kubo, J. Phys. Soc. Jpn. **43**, 811 (1977).
⁴S. Mukamel, Phys. Rep. **93**, 1 (1982).
⁵K. K. Rebane and P. M. Saari, J. Luminescence **12/13**, 23 (1976); K. K. Rebane, J. Luminescence **18/19**, 693 (1979).
⁶T. Takagahara, in *Relaxation of Elementary Excitations*, edited by R. Kubo and E. Hanamura (Springer-Verlag, Berlin, 1980), p. 45.
⁷T. Takagahara, in *Semiconductors Probed by Ultrafast Laser Spectroscopy*, edited by R. R. Alfano (Academic, New York, 1984), p. 331.

- ⁸M. Aihara, Solid State Commun. **53**, 437 (1985).
⁹R. G. DeVoe and R. G. Brewer, Phys. Rev. Lett. **50**, 1269 (1983).
¹⁰T. Takagahara, E. Hanamura, and R. Kubo, J. Phys. Soc. Jpn. **43**, 1522 (1977).
¹¹E. Hanamura and T. Takagahara, J. Phys. Soc. Jpn. **47**, 410 (1979).
¹²T. Takagahara, E. Hanamura, and R. Kubo, J. Phys. Soc. Jpn. **44**, 728 (1978).
¹³T. Takagahara, E. Hanamura, and R. Kubo, J. Phys. Soc. Jpn. **44**, 742 (1978).
¹⁴S. Mukamel, A. Ben-Reuven, and J. Jortner, Phys. Rev. A **12**, 947 (1975).
¹⁵A. Nakamura, M. Shimura, M. Hirai, and S. Nakashima, J. Phys. (Paris) Colloq. **C7**, 179 (1985).
¹⁶R. Kato and T. Sakai, Solid State Commun. **59**, 721 (1986).